Chemical Geology 641 (2023) 121777

Contents lists available at ScienceDirect

Chemical Geology

journal homepage: www.elsevier.com/locate/chemgeo

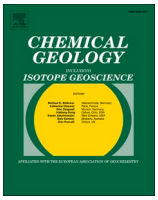

Mercury isotopic compositions of iron oxide-copper-gold (IOCG) hydrothermal systems: Deep Hg cycling in intracontinental settings

Xueqing Yin [a], Xinfu Zhao [a,*], Runsheng Yin [b], Lingjian Gao [b], Changzhou Deng [b], Zhendong Tian [b], Shengren Chang [a], Bernd Lehmann [c]

[a] State Key Laboratory of Geological Processes and Mineral Resources, School of Earth Resources, China University of Geosciences, Wuhan 430074, China
[b] State Key Laboratory of Ore Deposit Geochemistry, Institute of Geochemistry, Chinese Academy of Sciences, Guiyang 550081, China
[c] Mineral Resources, Technische Universität Clausthal, Clausthal-Zellerfeld 38678, Germany

ARTICLE INFO

Editor: Dr. Marco Fiorentini

Keywords:
Mercury isotopes
Iron oxide-copper-gold (IOCG) hydrothermal systems
Deep mercury cycling
Intracontinental setting

ABSTRACT

Mercury isotopes display unique mass-independent fractionation (MIF), typically expressed as Δ^{199}Hg, which relates to photochemical reactions occurring at Earth's surface. Pronounced Hg-MIF signals have been observed in various hydrothermal systems in both convergent margins and intracontinental settings, highlighting the recycling of Hg from marine or terrestrial reservoirs into shallow continental hydrothermal systems. However, the geochemical fate of Hg in deep continental environments of intracontinental settings remains poorly understood. Iron oxide-copper-gold (IOCG) hydrothermal systems typically involve the circulation of fluids from both deep magmatism and continental basins, providing an opportunity to investigate this issue. Here, we present the Hg isotopic compositions of ore minerals from five representative IOCG deposits in the Kangdian region, South China. All the studied ore samples display large mass-dependent fractionation with δ^{202}Hg of −3.23 to 1.06‰, but a relatively narrow range of Δ^{199}Hg of −0.17 to 0.11‰. These isotopic signatures support the hypothesis of binary mixing of Hg from two sources: (1) a magmatic endmember (~two thirds) derived from the lithospheric mantle with low δ^{202}Hg (−3 to −1‰) and near-zero Δ^{199}Hg, and (2) a crustal source (~one third) originating from the basement rocks with relatively higher δ^{202}Hg (−1 to 1‰) and negative Δ^{199}Hg (−0.2 to 0‰). Compared to the shallow Pb-Zn-Au-Sb hydrothermal systems which formed in intracontinental basins through the circulation of fluids in the upper crust, the Hg components (and by analogy, the ore metals) in the Kangdian IOCG system are dominated by a lithospheric mantle source. Our study sheds light on deep Hg cycling and confirms the Hg isotope tracer as a tool for revealing metal sources in hydrothermal ore systems.

1. Introduction

Mercury (Hg) is a heavy metal of great interest to geoscientists because its seven natural stable isotopes (196, 198–202, 204) display both large isotope mass-dependent fractionation (MDF, defined as δ^{202}Hg) and mass-independent fractionation (MIF, defined as Δ^{199}Hg, Δ^{200}Hg, and Δ^{201}Hg) (Bergquist and Blum, 2007). Hg-MDF occurs ubiquitously during many geological processes, however, Hg-MIF in natural samples is mainly produced during photochemical reactions with little interference from other processes (Blum et al., 2014). Photoreduction of Hg(II) has resulted in complementary Hg-MIF signals in Earth's surface systems, i.e., negative Δ^{199}Hg values (−0.6 to 0‰) in terrestrial systems (e.g., soil and vegetation) and positive Δ^{199}Hg values (0 to 0.4‰) in oceanic reservoirs (e.g., seawater and marine sediments) (e.g., Blum et al., 2014; Shen et al., 2019; Grasby et al., 2020; Kwon et al., 2020; Sun et al., 2023). The mantle and magmatic rocks without contributions from the surface systems have near-zero Δ^{199}Hg of 0.0 ± 0.1‰ (2SD, Moynier et al., 2021; Yin et al., 2022). Because magmatic, hydrothermal, and/or metamorphic processes do not trigger Hg-MIF (Deng et al., 2021a, 2021b, 2022a; Chen et al., 2022; Yin et al., 2022), Δ^{199}Hg signals can hence serve as a tracer for deep recycling processes in Earth's interior (Moynier et al., 2021; Wang et al., 2021; Deng et al., 2022b; Yin et al., 2022).

Given the strong affinity of Hg with ore metals (e.g., Cu, Au, Sb, Pb, and Zn), Hg-MIF signatures are particularly valuable in tracing metal sources of hydrothermal ore systems. Many studies have shown that Δ^{199}Hg values for hydrothermal ore systems in different geological settings are highly variable. For example, epithermal Au-Sb-Hg deposits

* Corresponding author.
E-mail address: xfzhao@cug.edu.cn (X. Zhao).

https://doi.org/10.1016/j.chemgeo.2023.121777
Received 29 June 2023; Received in revised form 29 September 2023; Accepted 8 October 2023
Available online 13 October 2023

in convergent margins mainly exhibit positive Δ^{199}Hg values (0 to 0.3‰), indicating the recycling of marine Hg reservoirs into arc-related hydrothermal systems via oceanic subduction (Deng et al., 2021a, 2021b). In contrast, sediment-hosted Pb-Zn-Au-Sb deposits of intracontinental settings from South China mainly display negative Δ^{199}Hg values, which have been attributed to the leaching and remobilization of Hg and ore metals from terrestrial sedimentary/basement rocks by basinal fluids (e.g., Xu et al., 2018; Fu et al., 2020; Liu et al., 2021; Deng et al., 2022b, 2022c; Gao et al., 2023). Overall, Δ^{199}Hg signals can potentially be used as a tracer for understanding Hg recycle and determining ore metal sources in hydrothermal systems. To date, available data on Hg cycling in intracontinental settings are mostly from shallow sediment-hosted hydrothermal systems; hydrothermal systems involving deep magmatism have not been studied yet.

Iron oxide-copper-gold (IOCG) deposits are a rare type of magmatic-hydrothermal deposits that were initially proposed for the giant Olympic Dam deposit and Cu-Au deposits in the Cloncurry region, Australia (e.g., Hitzman, 2000; Williams et al., 2005; Groves et al., 2010). They are commonly hosted within breccia bodies and are related to regional-scale hydrothermal circulation, which involves fluid mixing of both deep magmatism and shallow external sources (e.g., basinal brines and/or meteoric water). However, the origin of IOCG deposits, particularly the source of ore metals, is highly debated and two contrasting models are proposed: (1) a magmatic source from mafic rocks derived from the subcontinental lithospheric mantle and (2) a crustal source by leaching of metals from supracrustal and/or continental basement rocks (Sillitoe, 2003; Williams et al., 2005; Pollard, 2006; Groves et al., 2010; Xavier et al., 2012; Barton, 2014). Although different tectonic settings, including orogenic, post-orogenic, and back-arc settings, were proposed for the formation of IOCG deposits (Hitzman, 2000; Sillitoe, 2003; Williams et al., 2005; Groves et al., 2010), recent studies have suggested that IOCG deposits are associated with bimodal magmatism and the upwelling of mantle-derived magmas, indicating a regionally extensional event during ore formation in a back-arc or continental rifting setting (e.g., Groves et al., 2010; Chen et al., 2013a; Li et al., 2015; Zhao et al., 2017, 2019). The ~1.65 Ga IOCG deposits in the Kangdian metallogenic belt as a typical example have been shown to form in an intracontinental rift basin at the western Yangtze Block after its assembly into the Columbia supercontinent (Zhou et al., 2014; Zhao et al., 2019). Hence, they provide an excellent opportunity to explore the metal source of IOCG deposits and the deep Hg cycling in an intracontinental setting. Here we conducted Hg isotopic analyses of samples from five representative IOCG deposits in the Kangdian region, South China. Our data strongly argue for a predominant source of Hg and ore metals from the lithospheric mantle, with a lesser contribution from crustal rocks. This finding could also be widely applicable to other IOCG systems and related events in similar tectonic settings.

2. Geological setting

The South China Craton constitutes the Yangtze Block in the northwest and the Cathaysia Block in the southeast, which were amalgamated along the Jiangnan Orogen during the mid-Neoproterozoic (Fig. 1A).

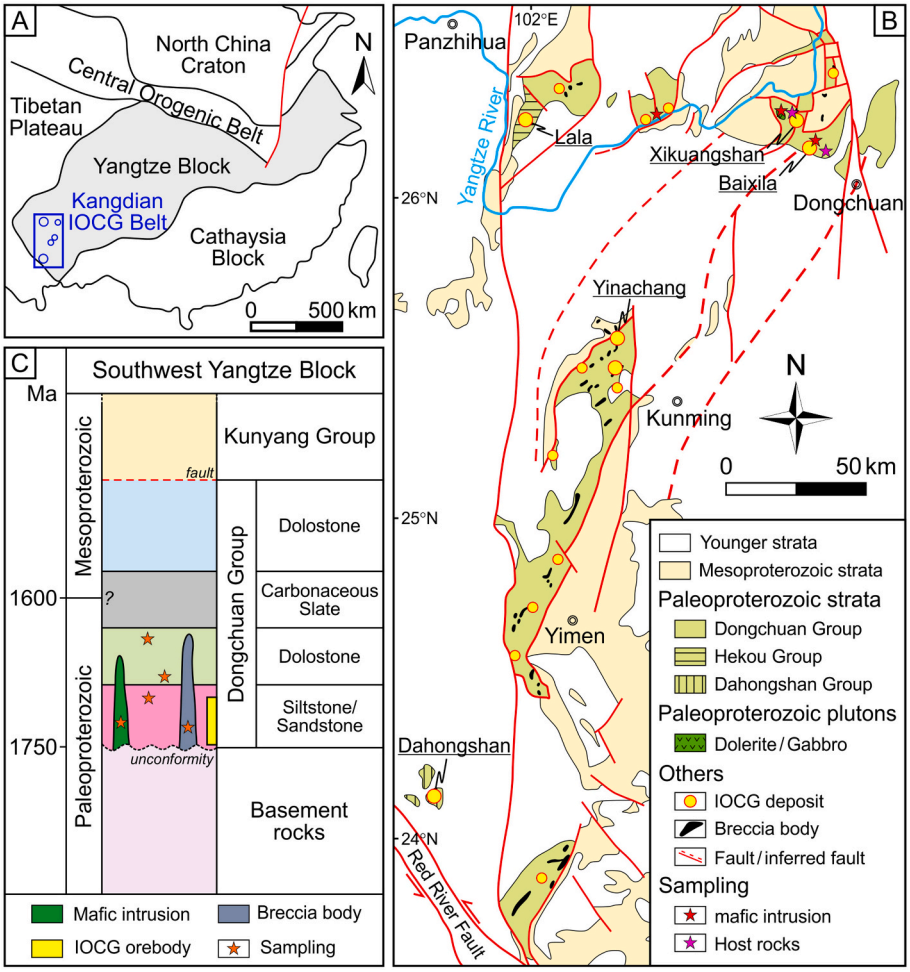

Fig. 1. (A) Sketch map of South China showing the location of Kangdian IOCG belt. Geologic map (B) and stratigraphic sequence (C) of the Kangdian IOCG belt showing the distribution of host rocks and IOCG deposits (modified from Zhao et al., 2019).

The southwestern part of the Yangtze Block has a thick sequence of fluvial to intertidal volcano-sedimentary rocks, known as the Dahongshan, Hekou, and Dongchuan groups, which formed in late Paleoproterozoic (~1.75 to 1.68 Ga) rift-related sedimentary basins (Fig. 1B, C, Zhao et al., 2010; Wang et al., 2014). They are composed of basal conglomerates, sandstones, and siltstones with minor tuffaceous and volcanic rocks, grading upward to interbedded carbonate rocks. These strata are locally intruded by slightly younger late Paleoproterozoic (1.69–1.65 Ga) mafic intrusions and late Mesoproterozoic mafic igneous rocks, all of which display geochemical affinities of intracontinental rift-related magmatic rocks (Zhou et al., 2014; Lu et al., 2020). In addition, mid-Neoproterozoic magmatism with ages between ~860 and ~740 Ma has produced large volumes of gabbroic, dioritic, and granitic intrusions, which have been interpreted to be products of either subduction-related or a mantle-plume origin (e.g., Zhou et al., 2002; Li et al., 2003).

More than twenty Fe-Cu deposits are hosted within the ~1.70 Ga metavolcano-sedimentary rocks in the Kangdian region (Fig. 1B, Zhao et al., 2019). The geology and metallogeny of these IOCG deposits have been previously described in detail (Zhao and Zhou, 2011; Chen and Zhou, 2012; Zhu and Sun, 2013; Zhou et al., 2014; Li et al., 2015; Zhao et al., 2017, 2019; Su et al., 2021). In brief, the IOCG orebodies are generally stratabound and/or structurally controlled, and often show a close spatial association with mafic intrusions and voluminous hydrothermal breccia bodies. These IOCG deposits all share a similar style of hydrothermal alteration and mineralization, including widespread pre-ore Na alteration, Ca-Fe alteration characterized by magnetite-dominated Fe-(REE) mineralization, K-Fe alteration with economic Cu-(Au-REE) mineralization dominated by chalcopyrite and pyrite, and post-ore Ca-Mg alteration. They have similar isotopic ages of ~1.65 to 1.66 Ga, coeval with the regional mafic magmatism. The ore deposits have significant economic value with a total resource of about 1000 Mt. Fe, 7 Mt. Cu, and 80 t Au (Zhou et al., 2014; Zhao et al., 2017, 2019).

3. Samples and methods

Samples of representative ores and host rocks were collected from five IOCG deposits (Lala, Yinachang, Dahongshan, Xikuangshan, and Baixila) in the Kangdian region (Fig. 1B, C). These samples include 22 ores (handpicked for magnetite, pyrite, and chalcopyrite), 8 sedimentary rocks, and 3 gabbroic rocks. Sample details are shown in Fig. 2 and Tables 1-2.

Total Hg (THg) concentrations and isotopic compositions of the samples were measured at the Institute of Geochemistry, Chinese Academy of Sciences, Guiyang, China, following the previously described protocols (Yin et al., 2016; Zerkle et al., 2020). In brief, Hg contents were determined by DMA-80 Mercury Analyzer, yielding Hg

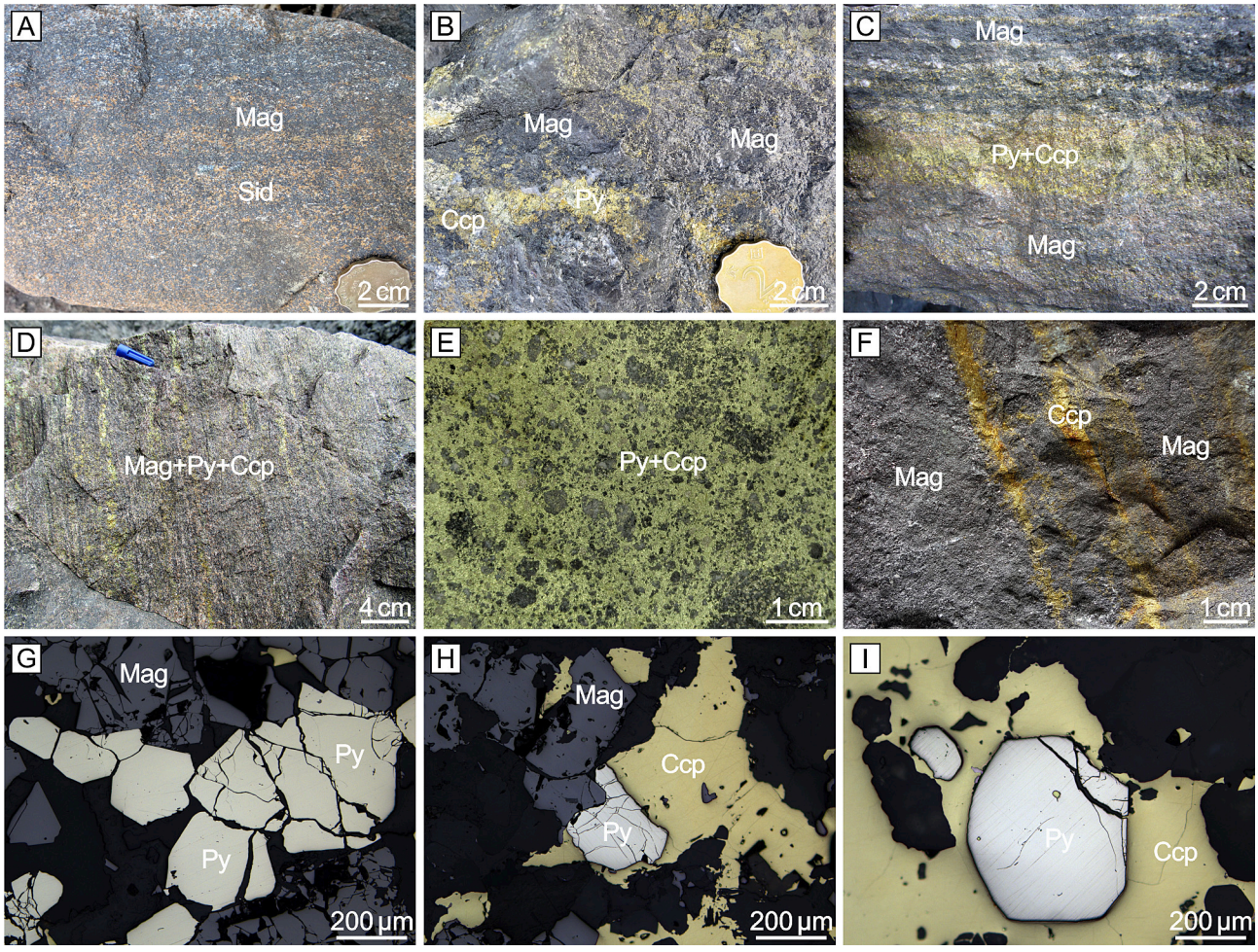

Fig. 2. Field photos and photomicrographs of representative ore samples. (A) Banded Fe ore and (B) massive Fe-Cu ore from the Dahongshan deposit. (C) Banded Fe-Cu ore from the Yinachang deposit. (D) Bedding-parallel banded Fe-Cu ore in altered siltstone and (E) high-grade massive sulfide ore from the Lala deposit. (F) massive Fe-Cu ore in the Baixila deposit. Representative photomicrographs (G-I) are from the Lala deposit. (G) Intergrowth of magnetite and pyrite in massive Fe-Cu ore. (H) Magnetite in the Ca-Fe alteration stage is texturally earlier than pyrite and chalcopyrite formed in the K-Fe alteration stage. (I) pyrite and chalcopyrite in the massive sulfide ore. Abbreviation: Mag-Magnetite, Ccp-Chalcopyrite, Py-Pyrite, Sid-Siderite.

Table 1
The characteristics of ore samples collected from the Kangdian IOCG belt in South China.

Sample No.	Descriptions	Minerals
Lala deposit		
LL21–17	High-grade massive Fe-Cu ore	Mag, Ccp
LL21–20	Disseminated ore in altered siltstone	Mag, Ccp
LL21–59	High-grade massive sulfide ore	Py, Ccp
LL21–72	Bedding-parallel banded ore in altered siltstone	Mag, Py, Ccp
Yinachang deposit		
YNC13–7	Massive chalcopyrite ore	Ccp
YNC13–8	Disseminated magnetite and chalcopyrite ore	Mag, Ccp
YNC13–12	Massive chalcopyrite ore	Ccp
YNC13–14	Massive chalcopyrite ore	Ccp
YNC13–24	Patched/disseminated Cu ore	Py, Ccp
Dahongshan deposit		
YN13–60	Banded Fe-Cu ore in altered siltstone	Py
DHS13–42	Garnet-biotite schist-hosted Fe-Cu ore	Mag, Ccp
DHS13–45	Massive Fe-Cu ore	Ccp
DHS15–137	Banded Fe-Cu ore in altered siltstone interbedded with dolostone	Mag, Ccp
DHS15–171	Banded Fe-Cu ore in altered siltstone interbedded with dolostone	Py
Baixila deposit		
LYN15–31	Massive Fe-Cu ore	Mag, Ccp
BXL16–2	Massive Fe-Cu ore	Mag, Ccp
BXL16–3	Massive Cu ore	Ccp
BXL-16	Disseminated Cu ore in altered siltstone	Ccp
BXL-19	Disseminated Cu ore in altered siltstone	Ccp
Xikuangshan deposit		
YMZ11–47	Hydrothermal breccia-hosted Cu ore	Ccp
YM19–11	Altered dolerite-hosted Cu ore	Ccp
YM20–01	Disseminated Fe-Cu ore in altered siltstone	Ccp

Note: Mag-magnetite, Py-Pyrite, Ccp-Chalcopyrite.

Table 2
The characteristics of mafic intrusions and host rocks collected from the Kangdian IOCG belt in South China.

Sample No.	Descriptions
Mafic intrusion	
DCW15–04	Gabbro in the Tangdan region
DCW15–58	Gabbro in the Xidianfang district
TAL16–29	Gabbro in the Tong'an region
Luoxue Formation	
DCW11–03	Dolostone in the upper Luoxue Formation
DCW11–30	Dolostone in the lower Luoxue Formation
DCW11–40	Dolostone in the lower Luoxue Formation
DCW11–51	Dolostone in the lower Luoxue Formation
Yinmin Formation	
YM19–52	Clast of least-altered siltstone in the Yinmin Breccia from the Yinmin ore district
YM20–06	Siltstone
YM20–08-1	Argillaceous siltstone
YM20–08-2	Calcareous siltstone

recoveries of 90–110% ($n = 6$) for GSS-4 soil standard reference material (SRM) and uncertainty of <10% for sample duplicates. These samples were processed by a double-stage tube furnace for preconcentration of Hg from the samples into 5 mL of 40% anti aqua regia (HNO_3/HCl = 2/1, *v/v*). The Hg-preconcentrated solution were diluted to 0.5 ng/mL Hg in 10–20% (*v/v*) acids using 18.2 MΩ•cm water and then measured using Neptune Plus multi-collector inductively coupled plasma mass spectrometry (MC-ICP-MS). Following the nomenclature recommended by Bergquist and Blum (2007), Hg-MDF is expressed in δ^{202}Hg notation in units of per mil (‰) referenced to the NIST-3133 Hg standard (analyzed before and after each sample):

$$\delta^{202}\mathrm{Hg}\ (‰) = \left[\left(^{202}\mathrm{Hg}/^{198}\mathrm{Hg}\right)_{\mathrm{sample}}/\left(^{202}\mathrm{Hg}/^{198}\mathrm{Hg}\right)_{\mathrm{standard}} - 1\right] \times 1000$$

Hg-MIF is reported in Δ notation, which describes the difference between the measured δ^{xxx}Hg and the theoretically predicted δ^{xxx}Hg value, in units of per mil (‰):

$$\Delta^{xxx}\mathrm{Hg} \approx \delta^{xxx}\mathrm{Hg} - \delta^{202}\mathrm{Hg} \times \beta$$

β is equal to 0.2520 for ^{199}Hg, 0.5024 for ^{200}Hg, and 0.7520 for ^{201}Hg. GSS-4 was prepared and measured in the same way as the samples. NIST-3177 secondary standard solutions, diluted to 0.5 ng/mL Hg in 10% HCl (*v/v*) were measured every 10 samples. The overall average and uncertainty of NIST-3177 (δ^{202}Hg: −0.48 ± 0.10‰; Δ^{199}Hg: −0.03 ± 0.04‰; Δ^{200}Hg: −0.01 ± 0.06‰; Δ^{201}Hg: −0.07 ± 0.03‰; 2SD, n = 5) and GSS-4 (δ^{202}Hg: −1.74 ± 0.11‰; Δ^{199}Hg: −0.48 ± 0.02‰; Δ^{200}Hg: −0.02 ± 0.05‰; Δ^{201}Hg: −0.42 ± 0.06‰; 2SD, n = 5) agree well with previous results (Bergquist and Blum, 2007; Blum et al., 2014; Deng et al., 2021b; Gao et al., 2022). The largest values of standard deviation (2SD) for NIST-3177 and GSS-4 were used to reflect analytical uncertainties.

4. Results

The analytical results are summarized in Table 3. As shown in Fig. 3, THg contents are generally low in the samples of sedimentary and igneous rocks, i.e., 3.11 to 23.4 ng/g for the ore-hosting clastic rocks, 6.94 to 13.4 ng/g for the hanging wall dolostones, and 7.13 to 7.55 ng/g for the gabbroic rocks. In contrast, ore minerals display THg concentrations (62.3 to 6540 ng/g) 1–2 orders of magnitude higher than the host rocks.

The clastic rocks, dolostones, and mafic intrusions have δ^{202}Hg values in the range of −1.93 to −1.09‰, −2.21 to −0.81‰, and −1.80 to −1.46‰, respectively, much smaller than those of the ore minerals (−3.23 to 1.06‰, Fig. 4A). The variation in Δ^{199}Hg of −0.17 to 0.11‰ is relatively small for all samples; besides a few outliers, most Δ^{199}Hg values fall into the range of −0.10 to 0.10‰ (Fig. 4A). There is a positive correlation between Δ^{201}Hg and Δ^{199}Hg (Δ^{199}Hg/Δ^{201}Hg = ~1, Fig. 4B) for all the data, which suggests Hg(II) photoreduction as the underlying process for the MIF signature (Blum et al., 2014).

5. Discussion

5.1. Two Hg sources in the Kangdian IOCG hydrothermal system

Since the discovery and definition of IOCG deposits, there have been many attempts to reveal the sources of ore metals and fluids, which are essential for developing a genetic model. Stable (e.g., H, B, C, O, and S) and radiogenic (e.g., Pb and Sr) isotopes are commonly adopted to trace the sources of ore metals and/or fluids. In recent years, non-traditional metal stable isotopes have been developed to gain new insights into the source of ore metals (e.g., Moynier et al., 2017; Zheng et al., 2019; Zhu et al., 2022; Mathur and Zhao, 2023). Mercury is the only metal displaying both significant Hg-MDF and Hg-MIF signals in natural samples (Blum et al., 2014). Similar to other metal isotopic systems, Hg-MDF mechanism is controlled by different geological processes (Blum et al., 2014), however, Hg-MIF signatures are predominantly controlled by photochemical reactions on Earth's surface and hence show a special advantage for tracing provenance regardless of magmatic, hydrothermal, and/or metamorphic processes (e.g., Deng et al., 2021a, 2021b, 2022a; Chen et al., 2022; Yin et al., 2022; Gao et al., 2023). Therefore, Hg isotopes can potentially provide important constraints on the metal sources in IOCG ore systems.

Mercury is a chalcophile metal, which is enriched in hydrothermal fluids, and can be ultimately incorporated into ore minerals. In this study, ore mineral samples contain Hg contents 2–3 orders higher than those of the host rocks. Neither native Hg nor independent Hg minerals

Table 3
THg concentrations and Hg isotopic compositions of samples collected from the Kangdian IOCG belt in South China.

Sample	Type	THg	δ^{199}Hg	δ^{200}Hg	δ^{201}Hg	δ^{202}Hg	Δ^{199}Hg	Δ^{200}Hg	Δ^{201}Hg
No.		ng/g	‰	‰	‰	‰	‰	‰	‰
Lala deposit									
LL21–17	Mag	1432.43	−0.56	−0.89	−1.40	−1.66	−0.14	−0.05	−0.15
LL21–20	Mag	364.33	−0.57	−1.01	−1.51	−1.98	−0.07	−0.02	−0.03
LL21–72	Mag	172.69	−0.46	−1.01	−1.51	−2.12	0.08	0.05	0.09
LL21–59	Py	1269.84	−0.71	−1.64	−2.37	−3.23	0.11	−0.02	0.06
LL21–59	Py^{R}	1481.98	−0.67	−1.51	−2.18	−2.98	0.08	−0.02	0.06
LL21–72	Py	495.97	−0.47	−0.91	−1.41	−1.78	−0.02	−0.01	−0.07
LL21–17	Ccp	2319.93	−0.53	−1.04	−1.52	−2.14	0.01	0.03	0.09
LL21–20	Ccp	3203.01	−0.57	−1.17	−1.67	−2.40	0.03	0.03	0.13
LL21–59	Ccp	2577.56	−0.50	−1.09	−1.62	−2.21	0.06	0.02	0.04
LL21–72	Ccp	692.76	−0.33	−0.69	−1.01	−1.44	0.03	0.03	0.07
Yinachang deposit									
YNC13–8	Mag	662.11	−0.59	−1.11	−1.70	−2.17	−0.04	−0.01	−0.06
YNC13–24	Py	1319.22	−0.13	−0.30	−0.43	−0.44	−0.02	−0.07	−0.09
YNC13–7	Ccp	491.70	−0.09	−0.13	−0.40	−0.33	0.00	0.04	−0.16
YNC13–8	Ccp	2819.13	−0.03	0.10	−0.02	0.17	−0.07	0.02	−0.14
YNC13–12	Ccp	496.30	−0.04	0.09	0.01	0.14	−0.07	0.02	−0.09
YNC13–14	Ccp	126.15	−0.19	−0.32	−0.56	−0.67	−0.02	0.02	−0.06
YNC13–24	Ccp	914.25	−0.18	−0.19	−0.40	−0.44	−0.07	0.03	−0.07
Dahongshan deposit									
DHS13–42	Mag	62.26	−0.48	−1.04	−1.56	−2.14	0.06	0.04	0.06
DHS15–137	Mag	1372.38	−0.59	−1.26	−1.95	−2.69	0.08	0.08	0.06
YN13–60	Py	624.09	−0.02	−0.16	−0.15	−0.29	0.05	−0.02	0.07
DHS15–171	Py	171.61	−0.49	−1.06	−1.48	−1.97	0.00	−0.07	0.00
DHS13–42	Ccp	274.07	0.09	0.24	0.33	0.46	−0.03	0.01	−0.01
DHS13–45	Ccp	833.33	−0.17	−0.05	−0.17	−0.04	−0.17	−0.03	−0.14
DHS15–137	Ccp	5284.90	−0.66	−1.35	−2.06	−2.58	−0.01	−0.05	−0.12
Baixila deposit									
LYN15–31	Mag	1399.55	−0.54	−1.02	−1.51	−2.01	−0.04	−0.02	0.00
BXL16–2	Mag	223.16	−0.30	−0.43	−0.79	−0.92	−0.07	0.03	−0.10
LYN15–31	Ccp	468.20	0.02	−0.08	−0.12	−0.16	0.06	0.00	0.00
BXL-16	Ccp	1468.25	0.06	0.08	0.01	0.09	0.04	0.04	−0.05
BXL-19	Ccp	734.19	0.31	0.56	0.86	1.06	0.05	0.02	0.06
BXL16–2	Ccp	973.94	−0.18	−0.26	−0.52	−0.53	−0.04	0.00	−0.12
BXL16–3	Ccp	2186.61	−0.21	−0.58	−0.89	−1.16	0.08	0.01	−0.02
Xikuangshan deposit									
YMZ11–47	Ccp	2635.80	−0.22	−0.34	−0.61	−0.65	−0.06	−0.01	−0.12
YM19–11	Ccp	593.75	−0.29	−0.42	−0.68	−0.83	−0.08	0.00	−0.06
YM20–01	Ccp	6540.28	−0.06	0.04	0.03	0.17	−0.10	−0.04	−0.10
Mafic intrusion									
DCW15–04	Gb	7.28	−0.29	−0.70	−1.09	−1.48	0.08	0.04	0.02
DCW15–58	Gb	7.13	−0.34	−0.73	−1.10	−1.46	0.03	0.00	−0.01
TAL16–29	Gb	7.55	−0.46	−0.90	−1.42	−1.80	−0.01	0.00	−0.07
Luoxue Formation									
DCW11–03	Dol	10.03	−0.25	−0.44	−0.78	−1.03	0.01	0.07	−0.01
DCW11–30	Dol	13.36	−0.21	−0.37	−0.66	−0.81	−0.01	0.04	−0.05
DCW11–40	Dol	12.01	−0.57	−1.11	−1.72	−2.21	−0.01	0.00	−0.06
DCW11–51	Dol	6.94	−0.43	−0.66	−1.09	−1.30	−0.10	−0.01	−0.11
Yinmin Formation									
YM19–52	Silt	23.35	−0.46	−0.96	−1.57	−1.93	0.02	0.01	−0.12
YM20–06	Silt	9.44	−0.21	−0.51	−0.86	−1.13	0.07	0.05	−0.01
YM20–08-1	Silt	3.11	−0.32	−0.58	−1.01	−1.09	−0.04	−0.03	−0.19
YM20–08-2	Silt	3.26	−0.42	−0.72	−1.28	−1.57	−0.03	0.07	−0.09

Note: Mag-magnetite, Py-Pyrite, Ccp-Chalcopyrite, Gb-Gabbro, Dol-Dolostone, Silt- Siltstone; R-Replicate sample.

have been observed in the studied deposits. The elevated Hg concentrations in ore samples can hence be attributed to the isomorphic substitution of Cu^{2+} and Fe^{2+} by Hg^{2+}, due to their similar geochemical properties during precipitation of hydrothermal minerals (Schwartz, 1997; Rytuba, 2003; Zhu et al., 2020; Deng et al., 2021a).

The δ^{202}Hg and Δ^{199}Hg values in our samples show different variations (Fig. 4A) and provide important insights into the source of Hg and ore metals in the Kangdian IOCG deposits. Most of the ore samples show negative δ^{202}Hg values of −3 to −1‰ and near-zero Δ^{199}Hg values of −0.1 to 0.1‰. These values fall within the range of the primitive mantle (0.0 ± 0.1‰, 2SD) (Moynier et al., 2021), and align with the values observed in the 1.69–1.65 Ga mafic intrusions (Fig. 4A). These intrusions, which are coeval with the Kangdian IOCG deposits, have been considered to be derived from the subcontinental lithospheric mantle

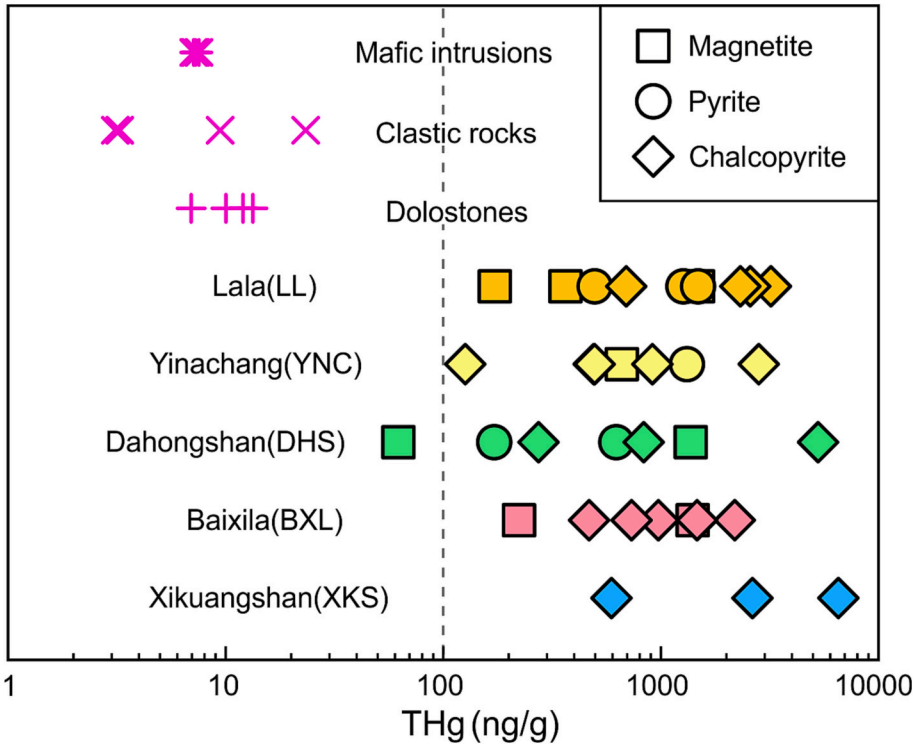

Fig. 3. THg concentration in ore minerals and host rocks in the Kangdian IOCG belt.

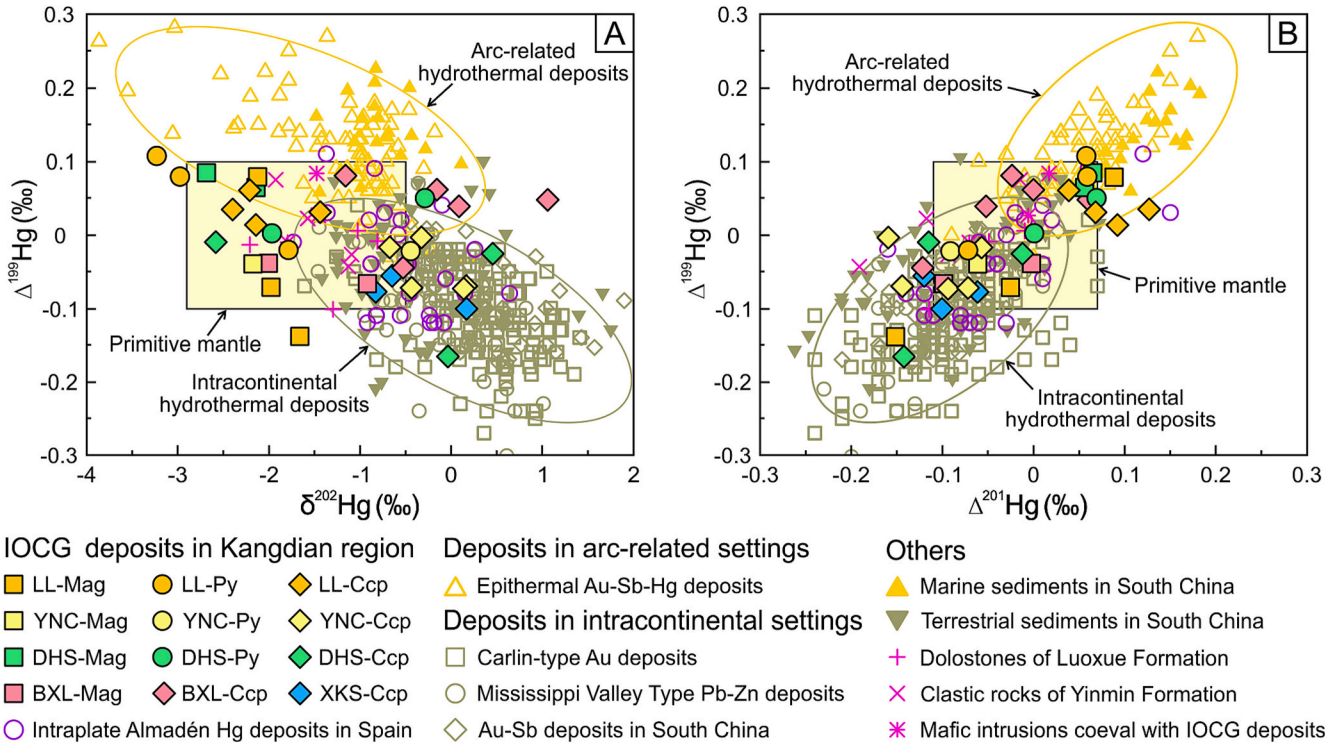

Fig. 4. $\Delta^{199}Hg$ versus $\delta^{202}Hg$ (A) and $\Delta^{199}Hg$ versus $\Delta^{201}Hg$ (B) diagrams. Hg isotopic data for arc-related Au-Sb-Hg deposits are from Deng et al. (2021a,b, and references therein), Carlin-type Au deposits are from Deng et al. (2022b) and Gao et al. (2023), MVT Pb-Zn deposits are from Liu et al. (2021) and Xu et al. (2018), Au-Sb deposits in South China are from Deng et al. (2022c) and Fu et al. (2020), Almadén Hg deposits in Spain are from Gray et al. (2013), and marine and terrestrial sediments in South China are from Deng et al. (2022a, c), Fu et al. (2020), Gao et al. (2023), and Xu et al. (2018). Refer to Fig. 3 for word abbreviation.

(Zhao et al., 2010; Chen et al., 2013b). Hence, we suggest that the ore metals of the IOCG deposits in the Kangdian region mainly originated from the subcontinental lithospheric mantle or their newly formed mafic rocks. In fact, previous studies on the Kangdian IOCG deposits have also revealed that they were essentially derived from magmatic-hydrothermal fluids (e.g., Zhao and Zhou, 2011; Chen et al., 2014; Li

et al., 2015; Zhao et al., 2017, 2019; Su et al., 2021). The boron isotope analyses on early-stage hydrothermal tourmalines in the Dahongshan deposit showed that the ore fluids were of magmatic origin. Moreover, in situ $^{87}Sr/^{86}Sr$ analyses on apatite grains from the Yinachang deposit yielded ratios from 0.70377 to 0.71074, which are broadly compatible with those of the coeval diabase intrusions (0.70592–0.70692) but show relatively large variations (reviewed by Zhao et al., 2019). Similar isotopic results were also reported for the apatite and carbonate minerals from the Lala deposit (Chen et al., 2014). In situ analyses of allanite and apatite from the Baixila deposit yielded ε_{Nd} values ranging from −2.8 to 0.3, which are roughly consistent with those of the contemporaneous igneous intrusions (−0.3 to 5.3) but significantly higher than those of the country rocks (−9.5 to −6.2), indicating REE components of ores were dominantly sourced from mantle-derived rocks (Su et al., 2021). Overall, both Hg isotopes of this study and previous isotopic data support the formation of the Kangdian IOCG ore system was related to a magmatic-hydrothermal event of regionally mantle-derived igneous rocks.

It is interesting to note that some ore mineral samples also show relatively high $\delta^{202}Hg$ values (> −1‰) and distinctly negative $\Delta^{199}Hg$ values (< −0.1‰) (Fig. 4A). Such samples also display a uniform $\Delta^{199}Hg/\Delta^{201}Hg$ ratio of ~1 (Fig. 4B), identical to that observed during the photoreduction of aqueous Hg (II) in surface environments (Blum et al., 2014), suggesting that a small fraction of Hg was likely sourced from recycled surface reservoirs. They have Hg isotopic signatures similar to those of the sediment-hosted Pb-Zn-Au-Sb deposits in intracontinental basins reported by previous studies (Fig. 4A), implying the involvement of terrestrial Hg in the formation of Kangdian IOCG deposits too. In addition, the basement rocks in South China show both positive $\delta^{202}Hg$ and negative $\Delta^{199}Hg$ values (e.g., Fu et al., 2020; Liu et al., 2021; Deng et al., 2022a, 2022b; Gao et al., 2023) and likely provide an additional Hg source for the studied IOCG deposits. Previous studies have also shown that these deposits display extensive hydrothermal alteration zones and basinal fluids were likely involved during the IOCG mineralization processes, as evidenced by a large range of $^{87}Sr/^{86}Sr$ values of apatite and carbonates, $\delta^{34}S$ values of sulfides, and $\delta^{11}B$ values of tourmaline at Cu-sulfides stage (reviewed by Zhao et al., 2019). Additionally, a genetic model of fluid mixing between magmatic and external fluids has been advocated for IOCG deposits in the Kangdian region and worldwide (Groves et al., 2010; Zhao et al., 2017, 2019). Therefore, we suggest that minor amount of Hg in sedimentary rocks and/or basement rocks was leached out during hydrothermal alteration and then introduced into the IOCG hydrothermal systems during large-scale fluid circulation.

5.2. Relative contribution of the two Hg sources

To quantitatively estimate the relative metal contribution of the subcontinental lithospheric mantle and basement rocks to the Kangdian IOCG hydrothermal system, we employed a two-endmember isotope mixing model using the $\Delta^{199}Hg$ values of ore minerals and different source endmembers:

$$f_s + f_b = 1.$$

$$f_s \times \Delta^{199}Hg_s + f_b \times \Delta^{199}Hg_b = \Delta^{199}Hg_i.$$

where f_s and f_b are the contribution fraction of the subcontinental lithospheric mantle and basement rocks, respectively. $\Delta^{199}Hg_s$, $\Delta^{199}Hg_b$, and $\Delta^{199}Hg_i$ are the mean isotopic values of the subcontinental lithospheric mantle, basement rocks, and ore minerals, respectively. Thereinto, the $\Delta^{199}Hg_s$ value of the subcontinental lithospheric mantle is represented by the studied gabbroic rocks. The $\Delta^{199}Hg_i$ value is calculated using ore minerals obtained in this study. Due to no outcrops of basement rocks in the Kangdian region and large-scale IOCG hydrothermal alteration, the $\Delta^{199}Hg_b$ value is roughly estimated by the terrestrial basement rocks in South China Craton. The model calculation was accomplished using the Python programming language. The Monte Carlo approach was performed to quantify the mean results and uncertainties of the mixing model. Because the method depends on random sampling and statistical data analysis, the Monte Carlo simulation was used to explore the potential results and their density by sampling the mean isotopic values ($\Delta^{199}Hg_s$, $\Delta^{199}Hg_b$, and $\Delta^{199}Hg_i$) with normal distribution (1σ) in 200 thousand simulations during 20 cycles. The modeling results are presented in Table 4.

We roughly estimated that the subcontinental lithospheric mantle and basement rocks contributed ~63 ± 8% and ~37 ± 8% (1SD) of the Hg, respectively, which by inference may also apply to other ore metals in the Kangdian IOCG systems. It should be noted that the $\Delta^{199}Hg_b$ value was likely overestimated in this study because a portion of terrestrial basement rocks have higher $\Delta^{199}Hg$ values due to sedimentation and deposition of terrestrial and coastal materials (e.g., Yin et al., 2015; Deng et al., 2022a; Gao et al., 2023). This scenario may result in larger $\Delta^{199}Hg_b$ values in our model calculation and therefore our modeling result represents the least estimation for the contribution proportion of the subcontinental lithospheric mantle to the Kangdian IOCG systems. In fact, the predominant Hg isotopic signature of the mantle source is also consistent with the conclusion that magmatic fluids are dominant in IOCG ore formation in Kangdian and worldwide (e.g., Groves et al., 2010; Simon et al., 2018; Zhao et al., 2017, 2019).

5.3. Hg recycling in intracontinental hydrothermal systems

Significant negative $\Delta^{199}Hg$ signatures have been observed in several sediment-hosted Pb-Zn-Au-Sb deposits in intracontinental sedimentary basins. In these deposits, Hg and ore metals were suggested to be mainly leached from continental basement rocks through basinal fluid circulation in shallow crustal environments (e.g., Fu et al., 2020; Liu et al., 2021; Deng et al., 2022b, 2022c; Gao et al., 2023). A recent study documented that minor samples of near-zero $\Delta^{199}Hg$ signatures were also present in sediment-hosted Au deposits, reflecting possibly minor Hg contribution from magmatic fluids too (Gao et al., 2023). However, different from these published data from shallow crustal levels, the Kangdian IOCG deposits mainly exhibit near-zero $\Delta^{199}Hg$ to slightly negative $\Delta^{199}Hg$ values, implying that the deep Hg cycling in intracontinental hydrothermal systems can be very different from that observed in Pb-Zn-Au-Sb systems within shallow crustal settings.

Considering the difference in Hg isotopic compositions and metal sources, in combination with the geotectonic evolution of the Kangdian paleo-rift basin, we propose a Hg cycling model at the lithospheric scale in an intracontinental setting (Fig. 5). During the Late Paleoproterozoic, the Kangdian region received long-term sedimentation and deposition of clastic sedimentary rocks in an intracontinental rift environment (Wang

Table 4
The results of binary mixing model using mercury isotopes.

Cycle No.	f_s	f_b
1	71.64	28.36
2	56.22	43.78
3	51.24	48.76
4	67.17	32.83
5	64.18	35.82
6	69.15	30.85
7	50.74	49.26
8	52.24	47.76
9	68.66	31.34
10	70.15	29.85
11	73.13	26.87
12	62.69	37.31
13	64.18	35.82
14	65.67	34.33
15	57.22	42.78
16	50.25	49.75
17	71.64	28.36
18	68.66	31.34
19	63.18	36.82
20	67.66	32.34

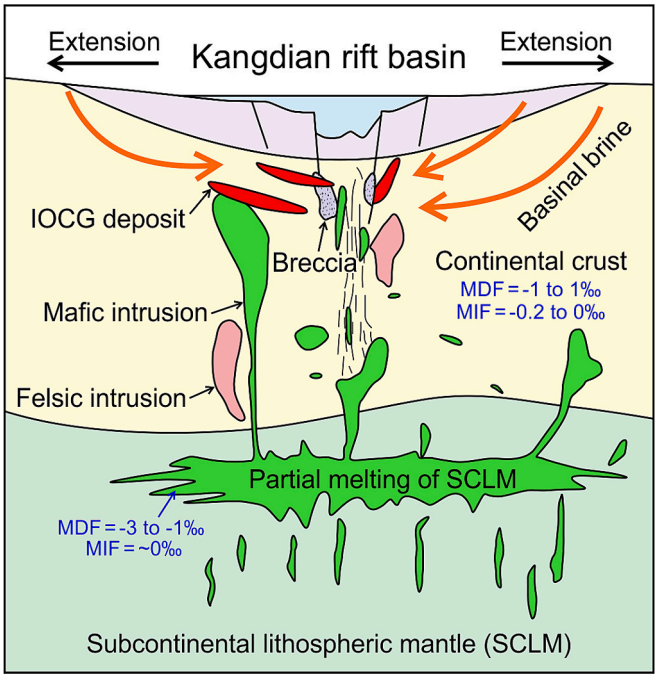

Fig. 5. Schematic diagram illustrating the deep Hg recycling in the Kangdian IOCG hydrothermal systems in an intracontinental rift setting.

et al., 2014), resulting in the accumulation of considerable amounts of terrestrial Hg in the sedimentary rock pile. These rocks were subsequently intruded by 1.69–1.65 Ga mafic intrusions, which are products of the partial melting of the lithospheric mantle in an extensional setting (Li et al., 2015; Zhao et al., 2019). The associated magmatic-hydrothermal fluids with near-zero Δ^{199}Hg signatures mixed with shallow basinal brines, whose circulation was set up by the heat of the mafic intrusions. The basinal brines scavenged Hg from the continental basement and the basin clastic sequence with negative Δ^{199}Hg signals. The IOCG ore systems incorporated Hg from both sources, with the deep source about two-thirds, and the shallow source about one-third of the total Hg budget. Such a scenario of multiple sources of Hg may also be applicable to other ore systems in intracontinental settings, such as the Almadén Hg deposits in Spain (e.g., Higueras et al., 2005; Gray et al., 2013) (Fig. 4).

6. Conclusions and implications

This study presents the first Hg isotopic data for IOCG hydrothermal systems, which are of importance to understanding the geochemical cycle of Hg in intracontinental rift settings. The IOCG ore systems have a mixed source signature with both lithospheric mantle and minor continental basement contributions to the Hg budget, which contrasts with sediment-hosted Pb-Zn-Au-Sb deposits of shallow crustal origin. As such, Hg isotopic compositions and cycling model in intracontinental hydrothermal systems can be various at different depths. Our results also suggest that Hg and other ore metals in IOCG ore systems were dominantly sourced from the lithosphere mantle and the deep mantle-derived Hg can be recycled and released into shallow crust through magmatic-hydrothermal mineralization processes. This study further highlights that Hg isotopes can be a useful proxy for understanding Hg cycling and can trace ore metals in hydrothermal ore systems.

Declaration of Competing Interest

The authors declare that they have no known competing financial interests or personal relationships that could have appeared to influence the work reported in this paper.

Data availability

Data will be made available on request.

Acknowledgments

This study was supported by the National Natural Science Foundation of China (U2202210, 42321001, and 41822203). We thank Dr. Wei Wang for generously providing the well-studied samples of dolostones and mafic rocks in this study. We appreciate Dr. Jian Wang, Dr. Zhikun Su, and Mr. Long Huang for their assistance during fieldwork, as well as Dr. Wenjie Shi and Mr. Yanyan Zhao for helping with sample preparation. We are grateful to Ms. Yi Deng for the Python programming language and discussion. We thank Dr. Marco Fiorentini for the editorial handling and comments, and Dr. Adam C. Simon and one anonymous reviewer for their constructive comments, which improved the quality of this paper.

References

Barton, M.D., 2014. Iron oxide (-Cu-Au-REE-P-Ag-U-Co) systems. In: Scott, S.D. (Ed.), Treatise on Geochemistry (second edition, volume 13). Elsevier, Amsterdam, pp. 515–541.

Bergquist, B.A., Blum, J.D., 2007. Mass-dependent and -independent fractionation of Hg isotopes by photoreduction in aquatic systems. Science 318, 417–420. https://doi.org/10.1126/science.1148050.

Blum, J.D., Sherman, L.S., Johnson, M.W., 2014. Mercury isotopes in Earth and environmental sciences. Annu. Rev. Earth Planet. Sci. 42, 249–269. https://doi.org/10.1146/annurev-earth-050212-124107.

Chen, W.T., Zhou, M.F., 2012. Paragenesis, stable isotopes, and molybdenite Re-Os isotope age of the Lala iron-copper deposit, southwest China. Econ. Geol. 107, 459–480. https://doi.org/10.2113/econgeo.107.3.459.

Chen, H., Cooke, D.R., Baker, M.J., 2013a. Mesozoic iron oxide copper-gold mineralization in the Central Andes and the Gondwana supercontinent breakup. Econ. Geol. 108, 37–44. https://doi.org/10.2113/econgeo.108.1.37.

Chen, W.T., Zhou, M.F., Zhao, X.F., 2013b. Late Paleoproterozoic sedimentary and mafic rocks in the Hekou area, SW China: implication for the reconstruction of the Yangtze Block in Columbia. Precambrian Res. 231, 61–77. https://doi.org/10.1016/j.precamres.2013.03.011.

Chen, W.T., Zhou, M.F., Gao, J.F., 2014. Constraints of Sr isotopic compositions of apatite and carbonates on the origin of Fe and Cu mineralizing fluids in the Lala Fe-Cu-(Mo, LREE) deposit. SW China. Ore Geol. Rev. 61, 96–106. https://doi.org/10.1016/j.oregeorev.2014.01.008.

Chen, D., Ren, D., Deng, C., Tian, Z., Yin, R., 2022. Mercury loss and isotope fractionation during high-pressure and high-temperature processing of sediments: implication for the behaviors of mercury during metamorphism. Geochim. Cosmochim. Acta. 334, 231–240. https://doi.org/10.1016/j.gca.2022.08.010.

Deng, C., Li, C., Rong, Y., Chen, D., Zhou, T., Wang, X., Chen, H., Lehmann, B., Yin, R., 2021a. Different metal sources in the evolution of an epithermal ore system: Evidence from mercury isotopes associated with the Erdaokan epithermal Ag-Pb-Zn deposit. NE China. Gondwana Res. 95, 1–9. https://doi.org/10.1016/j.gr.2021.03.010.

Deng, C., Sun, G., Rong, Y., Sun, R., Sun, D., Lehmann, B., Yin, R., 2021b. Recycling of mercury from the atmosphere-ocean system into volcanic-arc–associated epithermal gold systems. Geology. 49, 309–313. https://doi.org/10.1130/G48132.1.

Deng, C., Geng, H., Xiao, T., Chen, D., Sun, G., Yin, R., 2022a. Mercury isotopic compositions of the Precambrian rocks and implications for tracing mercury cycling in Earth's interior. Precambrian Res. 373, 106646 https://doi.org/10.1016/j.precamres.2022.106646.

Deng, C., Lehmann, B., Xiao, T., Tan, Q., Chen, D., Tian, Z., Wang, X., Sun, G., Yin, R., 2022b. Intracontinental and arc-related hydrothermal systems display distinct δ^{202}Hg and Δ^{199}Hg features: Implication for large-scale mercury recycling and isotopic fractionation in different tectonic settings. Earth Planet. Sci. Lett. 593, 117646 https://doi.org/10.1016/j.epsl.2022.117646.

Deng, C., Zhang, J., Hu, R., Luo, K., Zhu, Y., Yin, R., 2022c. Mercury isotope constraints on the genesis of late Mesozoic Sb deposits in South China. Sci. China Earth Sci. 65, 1–13. https://doi.org/10.1007/s11430-021-9851-x.

Fu, S., Hu, R., Yin, R., Yan, J., Mi, X., Song, Z., Sullivan, N.A., 2020. Mercury and in situ sulfur isotopes as constraints on the metal and sulfur sources for the world's largest Sb deposit at Xikuangshan, southern China. Miner. Deposita. 55, 1353–1364. https://doi.org/10.1007/s00126-019-00940-1.

Gao, W., Hu, R., Wang, X., Yin, R., Bi, X., Xie, Z., Fu, S., Yan, J., 2023. Large-scale basement mobilization endows the giant Carlin-type gold mineralization in the Youjiang Basin, South China: Insights from mercury isotopes. Geol. Soc. Am. Bull. https://doi.org/10.1130/B36636.1. In press.

Gao, L., Long, T.M., Sun, D., Deng, C., Tian, Z., Song, X.Y., Yin, R., 2022. Crustal mercury addition into the giant Jinchuan Ni-Cu sulfide deposit, China, and its geological

implications. Geochem. Geophys. Geosyst. 23 https://doi.org/10.1029/2022GC010349 e2022GC010349.
Grasby, S.E., Liu, X., Yin, R., Ernst, R.E., Chen, Z., 2020. Toxic mercury pulses into late Permian terrestrial and marine environments. Geology. 48, 830–833. https://doi.org/10.1130/G47295.1.
Gray, J.E., Pribil, M.J., Higueras, P.L., 2013. Mercury isotope fractionation during ore retorting in the Almadén mining district. Spain. Chem. Geol. 357, 150–157. https://doi.org/10.1016/j.chemgeo.2013.08.036.
Groves, D.I., Bierlein, F.P., Meinert, L.D., Hitzman, M.W., 2010. Iron oxide copper-gold (IOCG) deposits through Earth history: Implications for origin, lithospheric setting, and distinction from other epigenetic iron oxide deposits. Econ. Geol. 105, 641–654. https://doi.org/10.2113/gsecongeo.105.3.641.
Higueras, P., Munhá, J., Oyarzun, R., Tassinari, C.C., Ruiz, I.R., 2005. First lead isotopic data for cinnabar in the Almadén district (Spain): implications for the genesis of the mercury deposits. Miner. Deposita. 40, 115–122. https://doi.org/10.1007/s00126-005-0471-2.
Hitzman, M.W., 2000. Iron oxide-Cu-Au deposits: What, where, when and why. In: Porter, T.M. (Ed.), Hydrothermal iron oxide copper-gold and related deposits: a global perspective (volume 1). PGC Publishing, Adelaide, pp. 9–25.
Kwon, S.Y., Blum, J.D., Yin, R., Tsui, M.T.K., Yang, Y.H., Choi, J.W., 2020. Mercury stable isotopes for monitoring the effectiveness of the Minamata Convention on Mercury. Earth Sci. Rev. 203, 103111 https://doi.org/10.1016/j.earscirev.2020.103111.
Li, X.H., Li, Z.X., Ge, W., Zhou, H., Li, W., Liu, Y., Wingate, M.T., 2003. Neoproterozoic granitoids in South China: crustal melting above a mantle plume at ca. 825 Ma? Precambrian Res. 122, 45–83. https://doi.org/10.1016/S0301-9268(02)00207-3.
Li, X., Zhao, X., Zhou, M.F., Chen, W.T., Chu, Z., 2015. Fluid inclusion and isotopic constraints on the origin of the Paleoproterozoic Yinachang Fe-Cu-(REE) deposit, Southwest China. Econ. Geol. 110, 1339–1369. https://doi.org/10.2113/econgeo.110.5.1339.
Liu, Y.F., Qi, H.W., Bi, X.W., Hu, R.Z., Qi, L.K., Yin, R.S., Tang, Y.Y., 2021. Mercury and sulfur isotopic composition of sulfides from sediment-hosted lead-zinc deposits in Lanping basin. Southwestern China. Chem. Geol. 559, 119910 https://doi.org/10.1016/j.chemgeo.2020.119910.
Lu, G.M., Wang, W., Cawood, P.A., Ernst, R.E., Raveggi, M., Huang, S.F., Xue, E.K., 2020. Late Paleoproterozoic to Early Mesoproterozoic mafic magmatism in the SW Yangtze Block: Mantle plumes associated with Nuna Breakup? J. Geophys. Res.: Solid Earth. 125 https://doi.org/10.1029/2019JB019260 e2019JB019260.
Mathur, R., Zhao, Y., 2023. Copper isotopes used in mineral exploration. In: Huston, D., Gutzmer, J. (Eds.), Isotopes in Economic Geology, Metallogenesis and Exploration. Springer International Publishing, Cham, pp. 433–450.
Moynier, F., Jackson, M.G., Zhang, K., Cai, H., Halldórsson, S.A., Pik, R., Day, J.M., Chen, J., 2021. The mercury isotopic composition of Earth's mantle and the use of mass independently fractionated Hg to test for recycled crust. Geophys. Res. Lett. 48 https://doi.org/10.1029/2021GL094301 e2021GL094301.
Moynier, F., Vance, D., Fujii, T., Savage, P., 2017. The isotope geochemistry of zinc and copper. Rev. Mineral. Geochem. 82, 543–600. https://doi.org/10.2138/rmg.2017.82.13.
Pollard, P.J., 2006. An intrusion-related origin for Cu–Au mineralization in iron oxide–copper–gold (IOCG) provinces. Miner. Deposita. 41, 179–187. https://doi.org/10.1007/s00126-006-0054-x.
Rytuba, J.J., 2003. Mercury from mineral deposits and potential environmental impact. Environ. Geol. 43, 326–338. https://doi.org/10.1007/s00254-002-0629-5.
Schwartz, M.O., 1997. Mercury in zinc deposits: Economic geology of a polluting element. Int. Geol. Rev. 39, 905–923. https://doi.org/10.1080/00206819709465309.
Shen, J., Algeo, T.J., Chen, J., Planavsky, N.J., Feng, Q., Yu, J., Liu, J., 2019. Mercury in marine Ordovician/Silurian boundary sections of South China is sulfide-hosted and non-volcanic in origin. Earth Planet. Sci. Lett. 511, 130–140. https://doi.org/10.1016/j.epsl.2019.01.028.
Sillitoe, R.H., 2003. Iron oxide-copper-gold deposits: an Andean view. Miner. Deposita. 38, 787–812. https://doi.org/10.1007/s00126-003-0379-7.
Simon, A.C., Knipping, J., Reich, M., Barra, F., Deditius, A.P., Bilenker, L., Childress, T., 2018. Kiruna-type iron oxide-apatite (IOA) and iron oxide copper-gold (IOCG) deposits form by a combination of igneous and magmatic-hydrothermal processes: Evidence from the Chilean iron belt. In: Arribas, A.M., Mauk, J.L. (Eds.), Metals, Minerals, and Society (Special Publication 21). Society of Economic Geologists, Littleton, pp. 89–114.
Su, Z.K., Zhao, X.F., Li, X.C., Zhou, M.F., Kennedy, A.K., Zi, J.W., Spandler, C., Yang, Y.H., 2021. Unraveling mineralization and multistage hydrothermal overprinting histories by integrated in situ U-Pb and Sm-Nd isotopes in a Paleoproterozoic breccia-hosted IOCG deposit, SW China. Econ. Geol. 116, 1687–1710. https://doi.org/10.5382/econgeo.4840.
Sun, R., Liu, Y., Sonke, J.E., Zhang, F., Zhao, Y., Zhang, Y., Chen, J., Liu, C.Q., Shen, S., Anbar, A.D., Zheng, W., 2023. Mercury isotope evidence for marine photic zone euxinia across the end-Permian mass extinction. Commun. Earth Environ. 4, 159. https://doi.org/10.1038/s43247-023-00821-6.
Wang, W., Zhou, M.F., Zhao, X.F., Chen, W.T., Yan, D.P., 2014. Late Paleoproterozoic to Mesoproterozoic rift successions in SW China: implication for the Yangtze Block–North Australia–Northwest Laurentia connection in the Columbia supercontinent. Sediment. Geol. 309, 33–47. https://doi.org/10.1016/j.sedgeo.2014.05.004.
Wang, X., Deng, C., Yang, Z., Zhu, J.J., Yin, R., 2021. Oceanic mercury recycled into the mantle: evidence from positive Δ^{199}Hg in lamprophyres. Chem. Geol. 584, 120505 https://doi.org/10.1016/j.chemgeo.2021.120505.
Williams, P.J., Barton, M.D., Johnson, D.A., Fontboté, L., De Haller, A., Mark, G., Oliver, N.H., Marschik, R., 2005. Iron oxide copper-gold deposits: Geology, space-time distribution, and possible modes of origin. In: Hedenquist, J.W., Thompson, J.F., Goldfarb, R.J., Richards, J.P. (Eds.), Economic Geology 100th Anniversary Volume. Society of Economic Geologists, Littleton, pp. 515–541.
Xavier, R.P., Monteiro, L.V.S., Moreto, C.P.N., Pestilho, A.L.S., de Melo, G.H.C., da Silva, M.A.D., Aires, B., Ribeiro, C., Silva, F.H.F., 2012. The iron oxide copper-gold systems of the Carajás mineral province, Brazil. In: Hedenquist, J.W., Harris, M., Camus, F. (Eds.), Geology and Genesis of Major Copper Deposits and Districts of the World: A Tribute to Richard H. Sillitoe (Special Publication 16). Society of Economic Geologists, Littleton, pp. 433–453.
Xu, C., Yin, R., Peng, J., Hurley, J.P., Lepak, R.F., Gao, J., Feng, X., Hu, R., Bi, X., 2018. Mercury isotope constraints on the source for sediment-hosted lead-zinc deposits in the Changdu area, southwestern China. Miner. Deposita. 53, 339–352. https://doi.org/10.1007/s00126-017-0743-7.
Yin, R., Feng, X., Chen, B., Zhang, J., Wang, W., Li, X., 2015. Identifying the sources and processes of mercury in subtropical estuarine and ocean sediments using Hg isotopic composition. Environ. Sci. Technol. 49, 1347–1355. https://doi.org/10.1021/es504070y.
Yin, R., Krabbenhoft, D.P., Bergquist, B.A., Zheng, W., Lepak, R.F., Hurley, J.P., 2016. Effects of mercury and thallium concentrations on high precision determination of mercury isotopic composition by Neptune Plus multiple collector inductively coupled plasma mass spectrometry. J. Anal. At. Spectrom. 31, 2060–2068. https://doi.org/10.1039/C6JA00107F.
Yin, R., Chen, D., Pan, X., Deng, C., Chen, L., Song, X., Yu, S., Zhu, C., Wei, X., Xu, Y., Feng, X., Blum, J.D., Lehmann, B., 2022. Mantle Hg isotopic heterogeneity and evidence of oceanic Hg recycling into the mantle. Nat. Commun. 13, 948. https://doi.org/10.1038/s41467-022-28577-1.
Zerkle, A.L., Yin, R., Chen, C., Li, X., Izon, G.J., Grasby, S.E., 2020. Anomalous fractionation of mercury isotopes in the Late Archean atmosphere. Nat. Commun. 11, 1709. https://doi.org/10.1038/s41467-020-15495-3.
Zhao, X.F., Zhou, M.F., 2011. Fe–Cu deposits in the Kangdian region, SW China: a Proterozoic IOCG (iron-oxide–copper–gold) metallogenic province. Miner. Deposita. 46, 731–747. https://doi.org/10.1007/s00126-011-0342-y.
Zhao, X.F., Zhou, M.F., Li, J.W., Sun, M., Gao, J.F., Sun, W.H., Yang, J.H., 2010. Late Paleoproterozoic to early Mesoproterozoic Dongchuan Group in Yunnan, SW China: implications for tectonic evolution of the Yangtze Block. Precambrian Res. 182, 57–69. https://doi.org/10.1016/j.precamres.2010.06.021.
Zhao, X.F., Zhou, M.F., Su, Z.K., Li, X.C., Chen, W.T., Li, J.W., 2017. Geology, geochronology, and geochemistry of the Dahongshan Fe-Cu-(Au-Ag) deposit, Southwest China: Implications for the formation of iron oxide copper-gold deposits in intracratonic rift settings. Econ. Geol. 112, 603–628. https://doi.org/10.2113/econgeo.112.3.603.
Zhao, X.F., Chen, W.T., Li, X.C., Zhou, M.F., 2019. Iron oxide copper-gold deposits in China: A review and perspectives on ore genesis. In: Chang, Z., Goldfarb, R. (Eds.), Mineral Deposits of China (Special Publication 22). Society of Economic Geologists, Littleton, pp. 553–580.
Zheng, Y.C., Liu, S.A., Wu, C.D., Griffin, W.L., Li, Z.Q., Xu, B., Yang, Z.M., Hou, Z.Q., O'Reilly, S.Y., 2019. Cu isotopes reveal initial Cu enrichment in sources of giant porphyry deposits in a collisional setting. Geology 47, 135–138. https://doi.org/10.1130/G45362.1.
Zhou, M.F., Yan, D.P., Kennedy, A.K., Li, Y., Ding, J., 2002. SHRIMP U–Pb zircon geochronological and geochemical evidence for Neoproterozoic arc-magmatism along the western margin of the Yangtze Block, South China. Earth Planet. Sci. Lett. 196, 51–67. https://doi.org/10.1016/S0012-821X(01)00595-7.
Zhou, M.F., Zhao, X.F., Chen, W.T., Li, X.C., Wang, W., Yan, D.P., Qiu, H.N., 2014. Proterozoic Fe–Cu metallogeny and supercontinental cycles of the southwestern Yangtze Block, southern China and northern Vietnam. Earth Sci. Rev. 139, 59–82. https://doi.org/10.1016/j.earscirev.2014.08.013.
Zhu, Z., Sun, Y., 2013. Direct Re-Os dating of chalcopyrite from the Lala IOCG deposit in the Kangdian copper belt. China. Econ. Geol. 108, 871–882. https://doi.org/10.2113/econgeo.108.4.871.
Zhu, C., Tao, C., Yin, R., Liao, S., Yang, W., Liu, J., Barriga, F.J., 2020. Seawater versus mantle sources of mercury in sulfide-rich seafloor hydrothermal systems, Southwest Indian Ridge. Geochim. Cosmochim. Acta. 281, 91–101. https://doi.org/10.1016/j.gca.2020.05.008.
Zhu, X., Wang, Z., Chen, H., 2022. Advances in isotope geochronology and isotope geochemistry: a preface. J. Earth Sci. 33, 1–4. https://doi.org/10.1007/s12583-021-1605-x.